

FROM FOG TO FAILURE: HOW DEHAZING CAN HARM CLEAR IMAGE OBJECT DETECTION

Ashutosh Kumar

School of Information
Rochester Institute of Technology
Rochester, NY 14623, USA
ak1825@cs.rit.edu

Aman Chadha *

Amazon Gen AI
Santa Clara, CA, USA
hi@aman.ai

ABSTRACT

This study explores the challenges of integrating human visual cue-based dehazing into object detection, given the selective nature of human perception. While human vision adapts dynamically to environmental conditions, computational dehazing does not always enhance detection uniformly. We propose a multi-stage framework where a lightweight detector identifies regions of interest (RoIs), which are then enhanced via spatial attention-based dehazing before final detection by a heavier model. Though effective in foggy conditions, this approach unexpectedly degrades the performance on clear images. We analyze this phenomenon, investigate possible causes, and offer insights for designing hybrid pipelines that balance enhancement and detection. Our findings highlight the need for selective preprocessing and challenge assumptions about universal benefits from cascading transformations. The implementation of the framework is available¹.

1 INTRODUCTION

Low-visibility conditions, such as rain, snow, fog, smoke, and haze, pose significant challenges for deep learning applications in autonomous vehicles, security and surveillance, maritime navigation, and agricultural robotics. Under these conditions, object detection models struggle due to reduced contrast and obscured features, leading to performance degradation. This study proposes a deep learning framework inspired by human visual perception to enhance object recognition in adverse visibility scenarios, particularly in foggy environments.

A key motivation for this work comes from the impact of poor visibility on airport operations, where disruptions in taxiing and docking cause delays and increase reliance on ground support. Limited staff availability exacerbates these issues, sometimes resulting in flight cancellations. While initially driven by airport challenges, the proposed framework applies broadly to various low-visibility scenarios across multiple domains.

To address these challenges, we introduce **Selective Region Enhancement**, a method that focuses on specific regions of interest rather than applying uniform dehazing. This approach reduces processing overhead and prevents unintended degradations that may introduce false positives. Additionally, we propose **Integration with Object Detection**, bridging image enhancement with object detection in a unified pipeline. This integration leverages the strengths of both techniques, overcoming limitations of traditional independent processing models. Our approach draws inspiration from human visual mechanisms, including selective attention, foveal and peripheral vision, adaptive eye responses, bottom-up sensory cues, and top-down goal-driven processing (see Appendix B).

The paper is structured as follows: Section 2 reviews prior work on low-visibility object detection and integration of human visual cues in deep learning applications. Section 3 presents our framework, including its vision-inspired design, data set selection, and experimental setup, followed by results and observed anomalies in Section 4.

*Work done outside position at Amazon Gen AI.

¹<https://github.com/ashu1069/perceptual-piercing>

2 RELATED WORK

Advancements in navigation and detection under low-visibility conditions have leveraged sensor fusion, visual cue integration, and computational techniques. Aircraft landing studies have explored sensor fusion of visible and virtual imagery (Liu et al., 2014) and visual-inertial navigation using runway features (Zhang et al., 2018). Multi-sensor fusion algorithms have improved odometry in GPS-denied environments (Khattak et al., 2019), while research on depth visualization has enhanced navigation and obstacle avoidance (Lieby et al., 2011). Synthetic Vision Systems and full-windshield Head-Up Displays aid drivers and pilots in low visibility (Kramer et al., 2014; Charissis & Papanastasiou, 2010). Image enhancement techniques for low-light conditions (Atom et al., 2020) and the fusion of visual cues with wireless communication improve road safety (Boban et al., 2012). Studies have also emphasized the role of geometrical shapes and colors in driving perception via Head-Up Displays (Zhan et al., 2023).

Despite these advances, challenges persist, including computational complexity (Zhang et al., 2018; Atom et al., 2020; Tang et al., 2022), performance issues under extreme conditions (Khattak et al., 2019; Boban et al., 2012), overfitting due to limited datasets (Zhang et al., 2018; Khattak et al., 2019), and insufficient real-world validation (Liu et al., 2014; Boban et al., 2012; Tang et al., 2022). Some works lack clarity in explanation or rigorous validation (Kramer et al., 2014; Zhan et al., 2023).

In visual recognition, research has explored human-like processing in computational models. Studies on brain mechanisms highlight hierarchical, feedforward object recognition (DiCarlo et al., 2012), while comparisons with deep neural networks (DNNs) reveal human superiority in handling distortions and attention mechanisms (Dodge & Karam, 2017; van Dyck et al., 2021). Eye-tracking data has been used to guide DNN attention with limited success (van Dyck et al., 2022). Approaches such as adversarial learning for feature discrimination (Yang et al., 2023a), biologically inspired top-down and bottom-up models (Malowany & Guterman, 2020), and retina-mimicking models for dehazing (Zhang et al., 2015) have been proposed. Foveal-peripheral dynamics have also been explored to balance computational efficiency and high-resolution perception (Lukanov et al., 2021).

Recent research has tackled low-visibility challenges like fog, low light, and sandstorms. The YOLOv5s FMG algorithm improves small-target detection with enhanced modules (Zheng et al., 2023), while novel MLP-based networks refine image clarity in hazy and sandstorm conditions (Gao et al., 2023). The PKAL approach integrates adversarial learning and feature priors for robust recognition (Yang et al., 2023b). Deformable convolutions and attention mechanisms enhance pedestrian and vehicle detection in poor visibility (Wu & Gao, 2023). Reviews highlight the limitations of non-learning and meta-heuristic dehazing methods in real-time applications (V et al., 2023), emphasizing the need for integrated low-level and high-level vision techniques (Yang et al., 2020). Innovations such as spatiotemporal attention for video sequences (Zhai & Shah, 2006), the PDE framework for simultaneous detection and enhancement (Li et al., 2022), spatial priors for saliency detection (Jian et al., 2021), and early visual cues for object boundary detection (Mély et al., 2016) further contribute to the field.

Despite advances, existing methods struggle with joint optimization of object detection and image enhancement, detection of low-contrast objects, and adaptation to dynamic visibility changes. This paper addresses these challenges by integrating human visual cues, such as attention mechanisms and contextual understanding, into object detection, enhancing both robustness and efficiency. Traditional approaches process entire images uniformly, increasing computational load, and sometimes degrading clear regions. Our method selectively enhances regions of interest, reducing unnecessary computations and improving responsiveness under varying conditions.

3 METHODOLOGY

The proposed methodology, illustrated in Figure 1, presents a deep learning framework that enhances object detection in low-visibility conditions by leveraging the atmospheric scattering model and human visual cortex principles. It integrates adaptive image enhancement with object detection, optimizing performance through different integration strategies. The pipeline starts with a lightweight detection model to identify regions of interest, guiding spatial attention in the dehaz-

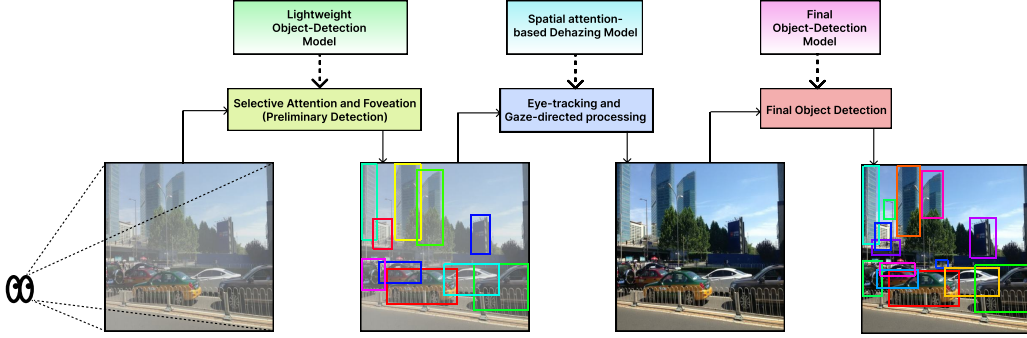


Figure 1: Overall architecture of Perceptual Piercing: (a) Preliminary detection using lightweight object detection model (b) Gaze-directed dehazing using spatial attention on region of interests (c) Final detection using a large and robust model.

ing process. This targeted enhancement preserves critical features while reducing computational overhead. A more robust detection model then refines and improves object recognition.

For dehazing, we train and evaluate state-of-the-art models, including AOD-Net(Li et al., 2017b), UNet-Dehaze(Zhou et al., 2024), and DehazeNet(Cai et al., 2016), using the Foggy Cityscapes dataset (Sakaridis et al., 2018) (see AppendixA). Table 2 presents a comparative analysis of their dehazing performance, while Figure 3 illustrates their impact on object detection. Among these methods, AOD-Net demonstrated the best dehazing performance, prompting further architectural enhancements. This resulted in AOD-NetX, a spatial attention-enhanced version trained on the Foggy Cityscapes dataset. Detailed modifications to AOD-NetX are provided in Appendix D.4 and Figure 2. For object detection models, we have used pre-trained YOLOv5 and YOLOv8 (see Appendix E).

To ensure robust evaluation, we tested our pipeline on three datasets: Foggy Cityscapes, RESIDE- β , and RESIDE-OTS (see Appendix A) (Li et al., 2019). This comprehensive assessment highlights the adaptability and effectiveness of our approach across multiple low-visibility scenarios.

4 RESULTS AND OBSERVED ANOMALIES

For in-distribution performance on the Foggy Cityscapes dataset, see Appendix F.1, while OOD evaluation on RESIDE- β (RTTS) and OTS datasets is detailed in Appendix F.2, demonstrating the pipeline’s robustness across diverse hazy conditions. Evaluation metrics include SSIM and PSNR for dehazing and mAP for object detection (Appendix G). Figure 4 illustrates visibility improvement with AOD-Net, Figure 5 shows its impact on object detection after dehazing with AOD-NetX on Foggy Cityscapes, and Figure 6 presents performance on the RESIDE dataset.

Table 1: Comparison of mean Average Precision (mAP) on clear and foggy conditions for different architecture variants. The performance change column quantifies the relative drop (red) or gain (green) in detection accuracy when transitioning from clear to foggy conditions.

Architecture Variants	mAP (Clear)	mAP (Foggy)	Performance Change
YOLOv5x	0.5644	0.4850	-14.07%
AOD-Net+YOLOv5x	0.6813	0.5822	-14.53%
YOLOv5s+AOD-NetX+YOLOv5x	0.4896	0.6152	+25.68%
YOLOv8x	0.5243	0.4948	-5.63%
AOD-Net+YOLOv8x	0.6099	0.5900	-3.27%
YOLOv8n+AOD-NetX+YOLOv8x	0.5150	0.6114	+18.71%

An unexpected finding in our evaluation is the performance trend of models incorporating AOD-NetX. The proposed pipeline performed superior on foggy images and while conventional models like YOLOv5x, YOLOv8x and also their integration with AOD-Net show a natural drop in mAP when transitioning from clear to foggy conditions, architectures integrating AOD-NetX exhibit an inverse trend—performing better under foggy conditions than in clear ones (see Table 1). Notably, **YOLOv5s+AOD-NetX+YOLOv5x** achieves a 25.68% relative mAP gain in foggy conditions, while **YOLOv8n+AOD-NetX+YOLOv8x** shows an 18.71% relative gain, highlighting the anomalies we found in our experiments.

5 DISCUSSIONS

The unexpected performance improvement of AOD-NetX-based models under foggy conditions (Table 1) raises critical questions about feature adaptation in hybrid object detection pipelines. Typically, object detectors exhibit a decline in accuracy when transitioning from clear to foggy conditions, as seen in conventional YOLOv5x and YOLOv8x models. However, our proposed AOD-NetX integration leads to an inverse trend—where object detection improves in foggy conditions relative to clear ones. This suggests that AOD-NetX introduces an implicit domain adaptation effect, making the detection network more attuned to foggy environments at the cost of generalization to clear images.

One possible explanation lies in dataset bias and overprocessing. Since AOD-NetX is trained primarily on foggy images, its learned feature space is optimized for haze removal but lacks the necessary constraints to preserve features in clear conditions. Consequently, when applied to clear images, the model introduces distortions instead of enhancements, disrupting feature consistency for the object detector. This emphasizes the need for context-aware enhancement, where image processing techniques are selectively applied based on scene conditions rather than indiscriminately.

Furthermore, the results challenge the assumption that cascading pipelines—where lightweight detection informs region-specific enhancement before a final robust detection—always improve performance. While effective in foggy settings, this multi-stage approach appears to introduce trade-offs, potentially harming accuracy in clear conditions. Future designs must strike a balance between specialization for adverse weather conditions and adaptability to diverse environments. Another consideration is the real-time feasibility of this approach. ROI-specific dehazing adds computational overhead, which could limit deployment in time-sensitive applications such as autonomous driving. Optimizing processing efficiency while retaining performance gains remains an open challenge.

6 LIMITATIONS & FUTURE WORK

A fundamental limitation of integrating dehazing into object detection is the feature space misalignment between foggy and clear images. Models trained primarily on foggy conditions lack the ability to preserve the natural characteristics of clear images, leading to unintended alterations that degrade detection performance. This highlights the importance of adaptive enhancement techniques that can determine when dehazing is necessary, rather than applying it universally. A potential solution is the integration of a haze-level estimation module, which could prevent unnecessary processing by triggering dehazing only when haze exceeds a certain threshold (Mao & Phommasak, 2014).

Another challenge is pretraining for scene differentiation. Since the AOD-NetX-enhanced models perform better in foggy conditions, their feature representations may be overfitting to haze-specific characteristics. Introducing joint training on both foggy and clear images could help mitigate this issue by aligning the feature space across different visibility conditions (Huang et al., 2024).

Additionally, unifying dehazing and object detection into a single model rather than having multi-stage framework may yield mutual benefits. For instance, detection-aware dehazing—where dehazing prioritizes regions of interest—could help the model preserve essential features for object detection, enhancing accuracy in both clear and foggy conditions (Fan et al., 2024).

Finally, computational efficiency remains a key concern for real-time applications. While the current pipeline enhances detection performance in low-visibility conditions, its multi-stage nature introduces latency. Future work should focus on optimizing inference speed, exploring lightweight

architectures, and developing efficient knowledge distillation techniques to maintain accuracy while reducing processing overhead.

By implementing **adaptive processing strategies**, **improved pretraining**, and **joint optimization**, future object detection pipelines can become more resilient across diverse visibility conditions, ensuring robust performance without compromising clarity in optimal conditions.

REFERENCES

Y. Atom, M. Ye, L. Ren, Y. Tai, and X. Liu. Color-wise attention network for low-light image enhancement. In *2020 IEEE/CVF Conference on Computer Vision and Pattern Recognition Workshops (CVPRW)*, pp. 2130–2139, Seattle, WA, USA, 2020. doi: 10.1109/CVPRW50498.2020.00261.

M. Boban, T. T. V. Vinhoza, O. K. Tonguz, and J. Barros. Seeing is believing—enhancing message dissemination in vehicular networks through visual cues. *IEEE Communications Letters*, 16(2): 238–241, February 2012. doi: 10.1109/LCOMM.2011.122211.112093.

Bolun Cai, Xiangmin Xu, Kui Jia, Chunmei Qing, and Dacheng Tao. Dehazenet: An end-to-end system for single image haze removal. *IEEE transactions on image processing*, 25(11):5187–5198, 2016.

Vassilis Charassis and Stylianos Papanastasiou. Human–machine collaboration through vehicle head up display interface. *Cognition, Technology Work*, 12:41–50, 2010. doi: 10.1007/s10111-008-0117-0.

J. J. DiCarlo, D. Zoccolan, and N. C. Rust. How does the brain solve visual object recognition? *Neuron*, 73(3):415–434, 2012. doi: 10.1016/j.neuron.2012.01.010.

S. Dodge and L. Karam. A study and comparison of human and deep learning recognition performance under visual distortions. In *2017 26th International Conference on Computer Communication and Networks (ICCCN)*, 2017. doi: 10.1109/icccn.2017.8038465.

Yihua Fan, Yongzhen Wang, Mingqiang Wei, Fu Lee Wang, and Haoran Xie. Friendnet: Detection-friendly dehazing network. *arXiv preprint arXiv:2403.04443*, 2024.

Y. Gao, W. Xu, and Y. Lu. Let you see in haze and sandstorm: Two-in-one low-visibility enhancement network. *IEEE Transactions on Instrumentation and Measurement*, 72:1–12, 2023. doi: 10.1109/TIM.2023.3304668.

Xiaochen Huang, Xiaofeng Wang, Qizhi Teng, Xiaohai He, and Honggang Chen. Degradation type-aware image restoration for effective object detection in adverse weather. *Sensors*, 24(19):6330, 2024.

M. Jian, J. Wang, H. Yu, G. Wang, X. Meng, L. Yang, J. Dong, and Y. Yin. Visual saliency detection by integrating spatial position prior of object with background cues. *Expert Systems With Applications*, 168:114219, 2021. doi: 10.1016/j.eswa.2020.114219.

S. Khattak, C. Papachristos, and K. Alexis. Visual-thermal landmarks and inertial fusion for navigation in degraded visual environments. In *2019 IEEE Aerospace Conference*, pp. 1–9, Big Sky, MT, USA, 2019. doi: 10.1109/AERO.2019.8741787.

L. J. Kramer et al. Using vision system technologies to enable operational improvements for low visibility approach and landing operations. In *2014 IEEE/AIAA 33rd Digital Avionics Systems Conference (DASC)*, pp. 2B2–1–2B2–17, Colorado Springs, CO, USA, 2014. doi: 10.1109/DASC.2014.6979422.

B. Li, X. Peng, Z. Wang, J. Xu, and D. Feng. Aod-net: All-in-one dehazing network. In *Proceedings of the IEEE international conference on computer vision*, pp. 4770–4778, 2017a.

B. Li et al. Benchmarking single-image dehazing and beyond. *IEEE Transactions on Image Processing*, 28(1):492–505, 2019. doi: 10.1109/TIP.2018.2867951.

Boyi Li, Xiulian Peng, Zhangyang Wang, Jizheng Xu, and Dan Feng. Aod-net: All-in-one dehazing network. In *Proceedings of the IEEE international conference on computer vision*, pp. 4770–4778, 2017b.

Zhiying Li, Shuyuan Lin, Zhongming Liang, Yongjia Lei, Zefan Wang, and Hao Chen. Pde: A real-time object detection and enhancing model under low visibility conditions. *International Journal of Advanced Computer Science and Applications(IJACSA)*, 13(12), 2022. doi: 10.14569/IJACSA.2022.0131299.

P. Lieby et al. Substituting depth for intensity and real-time phosphene rendering: Visual navigation under low vision conditions. In *2011 Annual International Conference of the IEEE Engineering in Medicine and Biology Society*, pp. 8017–8020, Boston, MA, USA, 2011. doi: 10.1109/IEMBS.2011.6091977.

C. Liu, Q. Zhao, Y. Zhang, and K. Tan. Runway extraction in low visibility conditions based on sensor fusion method. *IEEE Sensors Journal*, 14(6):1980–1987, June 2014. doi: 10.1109/JSEN.2014.2306911.

H. Lukanov, P. König, and G. Pipa. Biologically inspired deep learning model for efficient foveal-peripheral vision. *Frontiers in Computational Neuroscience*, 15, 2021. doi: 10.3389/fncom.2021.746204.

D. Malowany and H. Guterman. Biologically inspired visual system architecture for object recognition in autonomous systems. *Algorithms*, 13(7):167, 2020. doi: 10.3390/a13070167.

Jun Mao and Uthai Phommasak. Detecting foggy images and estimating the haze degree factor. *Journal of Computer Science & Systems Biology*, 7(06), 2014.

D. A. Mély, J. Kim, M. McGill, Y. Guo, and T. Serre. A systematic comparison between visual cues for boundary detection. *Vision Research*, 120:93–107, 2016. doi: 10.1016/j.visres.2015.11.007.

C. Sakaridis, D. Dai, and L. Van Gool. Semantic foggy scene understanding with synthetic data. *International Journal of Computer Vision*, 126:973–992, 2018. doi: 10.1007/s11263-018-1072-8.

Rong Tang, Qian Li, and Shaoen Tang. Comparison of visual features for image-based visibility detection. *Journal of Atmospheric and Oceanic Technology*, 39, 2022. doi: 10.1175/JTECH-D-21-0170.1.

S. Krishna B V, B. Rajalakshmi, U. Dhammini, M. K. Monika, C. Nethra, and K. Ashok. Image dehazing techniques for vision based applications - a survey. In *2023 International Conference for Advancement in Technology (ICONAT)*, pp. 1–5, Goa, India, 2023. doi: 10.1109/ICONAT57137.2023.10080156.

L. E. van Dyck, R. Kwitt, S. J. Denzler, and W. R. Gruber. Comparing object recognition in humans and deep convolutional neural networks: An eye-tracking study. *Frontiers in Neuroscience*, 15, 2021. doi: 10.3389/fnins.2021.750639.

L. E. van Dyck, S. J. Denzler, and W. R. Gruber. Guiding visual attention in deep convolutional neural networks based on human eye movements. *Frontiers in Neuroscience*, 16, 2022. doi: 10.3389/fnins.2022.975639.

X. Wu and Z. Gao. Based on the improved yolov8 pedestrian and vehicle detection under low-visibility conditions. In *2023 2nd International Conference on Artificial Intelligence and Intelligent Information Processing (AIIP)*, pp. 297–300, Hangzhou, China, 2023. doi: 10.1109/AIIP61647.2023.00063.

J. Yang, J. Yang, L. Luo, Y. Wang, S. Wang, and J. Liu. Robust visual recognition in poor visibility conditions: A prior knowledge-guided adversarial learning approach. *Electronics*, 12(17):3711, 2023a. doi: 10.3390/electronics12173711.

J. Yang, J. Yang, L. Luo, Y. Wang, S. Wang, and J. Liu. Robust visual recognition in poor visibility conditions: A prior knowledge-guided adversarial learning approach. *Electronics*, 12:3711, 2023b. doi: 10.3390/electronics12173711.

W. Yang et al. Advancing image understanding in poor visibility environments: A collective benchmark study. *IEEE Transactions on Image Processing*, 29:5737–5752, 2020. doi: 10.1109/TIP.2020.2981922.

Yun Zhai and Mubarak Shah. Visual attention detection in video sequences using spatiotemporal cues. In *Proceedings of the 14th ACM international conference on Multimedia (MM '06)*, pp. 815–824, New York, NY, USA, 2006. Association for Computing Machinery. doi: 10.1145/1180639.1180824.

Yu-Wei Zhan, Fan Liu, Xin Luo, Liqiang Nie, Xin-Shun Xu, and Mohan Kankanhalli. Generating human-centric visual cues for human-object interaction detection via large vision-language models. *arXiv*, 2023. arXiv:2311.16475.

L. Zhang, Z. Zhai, L. Bai, Y. Li, W. Niu, and L. Yuan. Visual-inertial state estimation for the civil aircraft landing in low visibility conditions. In *2018 International Conference on Networking and Network Applications (NaNA)*, pp. 292–297, Xi'an, China, 2018. doi: 10.1109/NANA.2018.8648726.

X.-S. Zhang, S.-B. Gao, C.-Y. Li, and Y.-J. Li. A retina inspired model for enhancing visibility of hazy images. *Frontiers in Computational Neuroscience*, 9, 2015. doi: 10.3389/fncom.2015.00151.

Y. Zheng, Y. Zhan, X. Huang, and G. Ji. Yolov5s fmg: An improved small target detection algorithm based on yolov5 in low visibility. *IEEE Access*, 11:75782–75793, 2023. doi: 10.1109/ACCESS.2023.3297218.

Hao Zhou, Zekai Chen, Qiao Li, and Tao Tao. Dehaze-unet: A lightweight network based on unet for single-image dehazing. *Electronics*, 13(11):2082, 2024.

A DATASETS

A.1 FOGGY CITYSCAPES

The Foggy Cityscapes (Sakaridis et al., 2018) dataset is created to address the problem of semantic foggy scene understanding (SFSU). While there has been extensive research on image dehazing and semantic scene understanding with clear-weather images, SFSU has received little attention. Due to the difficulty in collecting and annotating foggy images, synthetic fog is added to real images depicting clear-weather outdoor scenes. This synthetic fog generation leverages incomplete depth information to create realistic foggy conditions on images from the Cityscapes dataset, resulting in Foggy Cityscapes with 20,550 images. The training set consists of 2975 images, validated on 500 images, and the test set had 1525 images. The key features of the dataset include:

- **Synthetic Fog Generation:** Real clear-weather images are used, and synthetic fog is added using a complete pipeline that employs the transmission map.
- **Data Utilization:** The dataset can be utilized for supervised learning and semi-supervised learning. We generated a foggy dataset using the synthetic transmission map and then performed supervised learning on the synthetic foggy data.

A.2 RESIDE- β

The RESIDE- β Outdoor Training Set (OTS) is a comprehensive dataset designed to facilitate research in outdoor image dehazing. It addresses the challenges posed by haze in outdoor scenes, which significantly degrades image quality and affects subsequent tasks such as object detection and semantic segmentation. The dataset includes approximately 72,135 outdoor images with varying degrees of haze, enabling robust training of dehazing algorithms. For testing, we are using the RESIDE- β (REalistic Single Image DEhazing) dataset (Li et al., 2019). The subset of RESIDE- β , Real-Time Testing Set (RTTS) consists of 4,322 real-world hazy images with annotations for object detection. The training set consists of 3000 images, validated on 500 images, and the test set had 1500 images.

B HUMAN VISUAL CUES

Selective Attention and Foveation: The human eye is not equally sensitive to all parts of the visual field. Central vision, or foveal vision, is highly detailed and used for tasks like reading and identifying objects. Peripheral vision is less detailed and more sensitive to motion. The system scans the entire image (peripheral vision) similar to our preliminary detection phase. This will identify areas for a more detailed analysis (foveal vision), mimicking the human approach of not processing every detail with equal clarity but focusing on areas of interest.

Adaptation to environmental conditions: Just as the human visual system adapts to different lighting conditions and levels of visibility (such as adjusting to a dark room after being in bright sunlight), the adaptive dehazing method adjusts the intensity and focus of its processing based on the detection feedback and environmental context, analogous to the way human vision adjusts to ensure optimal perception under varying conditions.

Eye Tracking and Gaze-directed processing: Eye-tracking monitors where a person is looking (the gaze) and what draws attention. In visual processing, this is analogous to directing computational resources toward areas of interest, much like the proposed method focuses on dehazing and detailed detection of regions where objects are likely to be present. By analogy, the system pays more attention to certain parts of the image, just as a person would fixate on specific areas within their field of view when searching for something.

Integration of Bottom-up and Top-down processes: The human visual system uses both bottom-up signals (from sensory input) and top-down processes (based on knowledge, expectations, and current goals) to interpret scenes. The proposed model initially uses a bottom-up approach (object detection algorithms flagging potential areas of interest) followed by a top-down approach (focusing on dehazing efforts based on three flagged areas and previous learning), mirroring the complex interplay between sensory data and cognitive processes in human vision.

C METHODOLOGY

Preliminary Detection: Implement a lightweight, fast object detection algorithm such as YOLOv5s or YOLOv8n to quickly scan the image for potential regions of interest or active regions and flag those patches with a high likelihood of containing objects. The smaller versions of standard YOLO models are less accurate than their full-sized counterparts but significantly faster, making them ideal for preliminary detection.

Region-based dehazing: Apply dehazing algorithms specifically to those active regions identified in the preliminary detection phase. Considering the depth or level of haze, the method should adapt based on the characteristics of the detected regions

The proposed architecture of **AOD-NetX** in Figure 2 utilizes the transmission map created by the standard AOD-Net (Li et al., 2017a) and applies it within a spatial attention map module to produce an attention-focused transmission map. This spatial attention map is derived from the bounding boxes or Regions of Interest identified by the lightweight model (YOLOv5s/YOLOv8n) in our proposed method. A sigmoid layer follows, mapping the output probabilities to a range between 0 and 1. We opt not to use softmax in this context due to the independent significance of each bounding box.

D DEHAZING MODELS

D.1 AOD-NET

AOD-Net, or All-in-One Dehazing Network, is a convolutional neural network (CNN) designed to remove haze from images by directly reconstructing the clean image through an end-to-end approach. Unlike traditional methods that separately estimate transmission maps and atmospheric light, AOD-Net is based on a re-formulated atmospheric scattering model, enabling it to generate dehazed images without intermediate estimations. This lightweight architecture not only achieves superior performance in terms of Peak Signal-to-Noise Ratio (PSNR) and Structural Similarity Index (SSIM) but also enhances visual quality. Moreover, its design allows for easy integration into

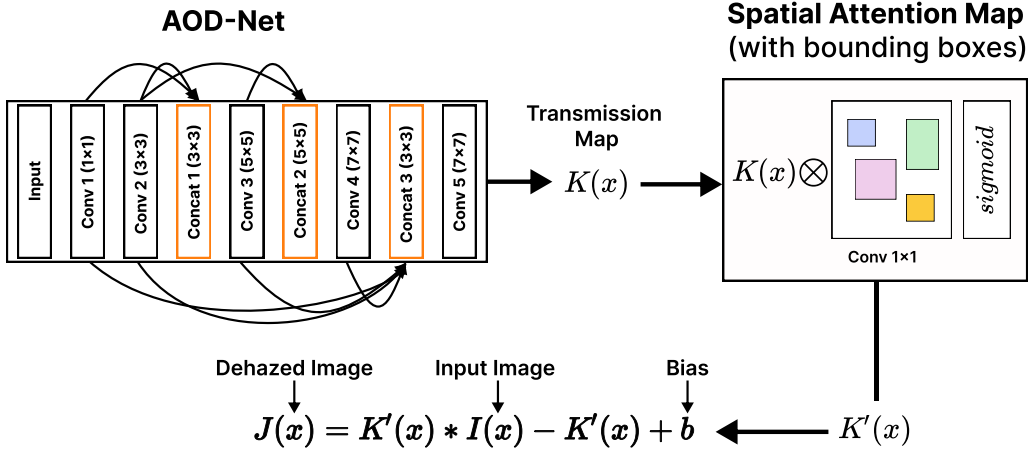


Figure 2: Architecture of AOD-NetX: The model takes the transmission map output, $K(x)$, from AOD-Net and applies a spatial attention layer to emphasize key regions of interest (bounding boxes) in the input image. The refined transmission map, $K'(x)$, is then utilized to dehaze the image.

other deep learning models, such as Faster R-CNN, improving performance on tasks like object detection in hazy conditions.

D.2 DEHAZE-UNET

The U-Net dehaze technique uses an encoder-decoder structure with skip connections for effective image dehazing. In the encoder, the network reduces spatial dimensions through double convolution layers, extracting essential features. Each convolution is followed by batch normalization and ReLU activation to enhance feature representation. In the decoder, these features are upsampled, reintegrating spatial details from the encoder via skip connections, crucial for restoring fine details lost in downsampling. Double convolution layers in the decoder refine the combined features, ensuring clarity. The model concludes with Max Pooling and Bilinear Interpolation, optimizing feature representation and smoothing transitions in the upsampled images, making U-Net highly effective in dehazing tasks.

D.3 DEHAZENET

The DehazeNet technique has four sequential steps presented in Figure 5 [35]. The feature extraction combines 16 filters with 4 MaxOut layers that perform max pooling to reduce data dimensionality [35]. Multi-scale mapping ensures that features of different complexity (both detailed and high-level features) are considered. Local extremum acts as max pooling that is specifically tuned to achieve spatial invariance, preserving the image resolution. In the final stage of Non-linear regression, the Bilateral ReLU is used as an activation function; it bounds the output within a specific range to avoid oversaturated regions.

D.4 AOD-NETX

The AOD-NetX architecture as shown in Figure 2 utilizes the transmission map created by the standard AOD-Net and applies it within a spatial attention map module to produce an attention-focused transmission map. This spatial attention map is derived from the bounding boxes or Regions of Interest identified by the lightweight model (YOLOv5s) in our proposed method. A sigmoid layer follows, mapping the output probabilities to a range between 0 and 1. We opt not to use softmax in this context due to the independent significance of each bounding box.

Table 2: Average Loss and SSIM scores of Dehazing techniques on Foggy Cityscapes dataset

Dehazing Model	Average Loss	SSIM
AOD-Net	0.0468	0.994
Dehaze-UNet	0.0323	0.992
DehazeNet	0.0572	0.991

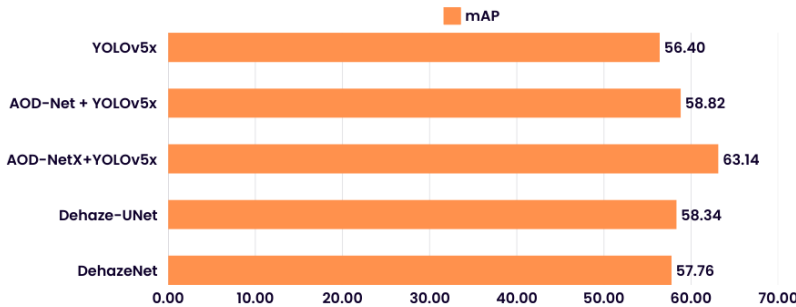


Figure 3: Comparison of mean Average Precision (mAP) for different dehazing and object detection module combinations.

E OBJECT DETECTION MODELS

The YOLO models used in the detection pipeline include a variety of versions optimized for different purposes. YOLOv5s is a lightweight variant designed for real-time detection with low computational requirements, while YOLOv8n (Nano) is tailored for high-speed applications on resource-constrained devices like mobile phones. On the other hand, YOLOv5x, with its CSP backbone and advanced data augmentation, provides enhanced performance for more complex scenes, and YOLOv8x (Extra Large) offers maximum accuracy for large-scale datasets. The detection process begins by using YOLOv5s or YOLOv8n on foggy images to generate initial annotations. These annotations, along with the original image, are then dehazed using AOD-NetX, and the dehazed image is subsequently passed through YOLOv5x or YOLOv8x for precise and refined detection results.

F ADDITIONAL RESULTS

The dehazing modules are trained separately on the provided datasets, while the object detection models (various YOLO versions) remain pre-trained on the MS-COCO dataset. This approach allows users to integrate the dehazing module with their own detection pipeline without requiring a complete re-training of the entire system. However, for improved results, the entire architecture could be fine-tuned on the target datasets, which would serve as a valuable direction for future ablation studies.

The results in Table 3 show that AOD-NetX generally outperforms the standard AOD-Net in terms of SSIM and PSNR across most datasets. For Foggy Cityscapes and RESIDE- β OTS, AOD-NetX achieves higher SSIM and PSNR, indicating improved structural similarity and signal quality. However, for RESIDE- β RTTS, while AOD-NetX has a slightly better PSNR, AOD-Net achieves a significantly higher SSIM score, suggesting that AOD-Net may retain more structural details in this particular dataset. Overall, AOD-NetX is more effective in most scenarios, especially for complex foggy conditions.

F.1 IN-DISTRIBUTION PERFORMANCE OF PERCEPTUAL PIERCING

The evaluation results of Perceptual Piercing variations trained and tested on the Foggy Cityscapes dataset has been provided in Table 4. The integration of dehazing modules, such as AOD-Net and

Table 3: Performance of dehazing methods: AOD-Net and AOD-NetX

Dataset	Dehazing Method	Evaluation Metrics	
		SSIM	PSNR
Foggy Cityscapes	AOD-Net	0.994	26.74
	AOD-NetX	0.998	27.22
RESIDE-β OTS	AOD-Net	0.920	24.14
	AOD-NetX	0.945	25.80
RESIDE-β RTTS	AOD-Net	0.932	27.59
	AOD-NetX	0.656	27.62

Table 4: **Train**- Foggy Cityscapes, **Test**- Foggy Cityscapes: Evaluation of various Perceptual Piercing variations based on mean Average Precision (mAP) under both clear and foggy conditions.

Architecture Variants	Conditions	Evaluation Metrics (mAP)
YOLOv5x	Clear	0.5644
	Foggy	0.485
AOD-Net+YOLOv5x	Clear	0.6813
	Foggy	0.5822
YOLOv5s+AOD-NetX+YOLOv5x	Clear	0.4896
	Foggy	0.6152
YOLOv8x	Clear	0.5243
	Foggy	0.4948
AOD-Net+YOLOv8x	Clear	0.6099
	Foggy	0.5900
YOLOv8n+AOD-NetX+YOLOv8x	Clear	0.5150
	Foggy	0.6114

AOD-NetX (detailed in Appendix C), consistently improves object detection in both clear and foggy conditions. The AOD-Net + YOLOv5x variant achieved the highest mAP under clear conditions (0.6813), while YOLOv5s + AOD-NetX + YOLOv5x and YOLOv8n + AOD-NetX + YOLOv8x performed best in foggy conditions, with mAP scores of 0.6152 and 0.6114, respectively. In contrast, baseline YOLO models (YOLOv5x and YOLOv8x) exhibited lower detection accuracy, underscoring the effectiveness of enhanced dehazing techniques in low-visibility environments.

F.2 OUT-OF-DISTRIBUTION PERFORMANCE OF PERCEPTUAL PIERCING

The evaluation of various Perceptual Piercing variations in Table 5 trained on Foggy Cityscapes and tested on RESIDE- β OTS and RTTS datasets shows that the YOLOv8x architecture achieved the highest mAP scores under foggy conditions, with 0.7125 on OTS and 0.6978 on RTTS. Among the YOLOv5 variants, the baseline YOLOv5x model performed the best, with 0.6944 on OTS and 0.6655 on RTTS. The addition of AOD-Net generally improved performance for YOLOv8 but had a diminishing effect on YOLOv5. Models incorporating AOD-NetX showed lower mAP values across both test datasets, indicating that its integration may need further optimization. Overall, the results suggest that YOLOv8x is more robust for foggy conditions compared to other variations.

G EVALUATION METRICS

G.1 STRUCTURAL SIMILARITY INDEX MEASURE (SSIM)

The performance of dehazing methods is evaluated by the following equation of SSIM score between two images:

$$SSIM(x, y) = \frac{(2\mu_x\mu_y + c_1)(2\sigma_{xy} + c_2)}{(\mu_x^2 + \mu_y^2 + c_1)(\sigma_x^2 + \sigma_y^2 + c_2)} \quad (1)$$

Table 5: **Train-** Foggy Cityscapes, **Test-** RESIDE- β OTS and RTTS: Evaluation of various Perceptual Piercing variations based on mean Average Precision (mAP) under foggy conditions.

Architecture Variants	Configuration	Evaluation Metrics (mAP)
YOLOv5x	Test: OTS	0.6944
	Test: RTTS	0.6655
AOD-Net+YOLOv5x	Test: OTS	0.6325
	Test: RTTS	0.6156
YOLOv5s+AOD-NetX+YOLOv5x	Test: OTS	0.5679
	Test: RTTS	0.5297
YOLOv8x	Test: OTS	0.7125
	Test: RTTS	0.6978
AOD-Net+YOLOv8x	Test: OTS	0.6458
	Test: RTTS	0.6125
YOLOv8n+AOD-NetX+YOLOv8x	Test: OTS	0.5779
	Test: RTTS	0.5312

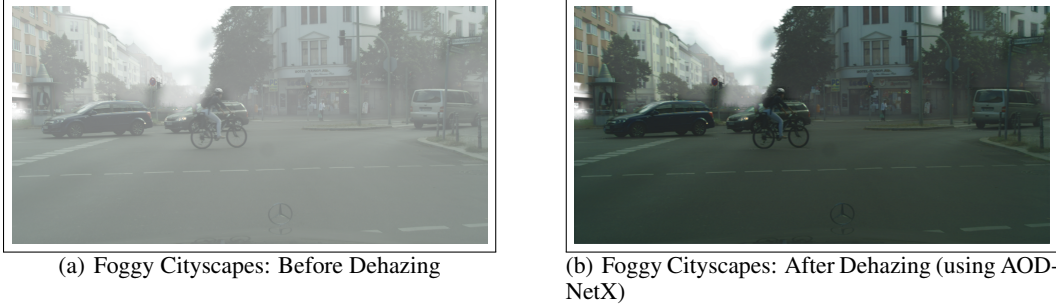


Figure 4: Dehazing performance on Foggy Cityscapes dataset.

where:

- μ_x and μ_y are the average of x and y respectively.
- σ_x^2 and σ_y^2 are the variance of x and y respectively.
- σ_{xy} is the covariance of x and y .
- $c_1 = (k_1 L)^2$ and $c_2 = (k_2 L)^2$ are two variables to stabilize the division with weak denominator; L is the dynamic range of the pixel-values (typically this is $2^{bits_per_pixel} - 1$), $k_1 = 0.01$ and $k_2 = 0.03$ by default.

G.2 PEAK SIGNAL-TO-NOISE RATIO (PSNR)

Peak Signal-to-Noise Ratio (PSNR) is a widely used metric for evaluating the quality of reconstructed images or videos compared to the original, reference data. It is expressed in decibels (dB) and is calculated based on the mean squared error (MSE) between the original and the reconstructed images. The formula for PSNR is given by:

$$\text{PSNR} = 10 \cdot \log_{10} \left(\frac{\text{MAX}^2}{\text{MSE}} \right), \quad (2)$$

where MAX is the maximum possible pixel value of the image (for example, 255 for 8-bit images), and MSE is the mean squared error, defined as:

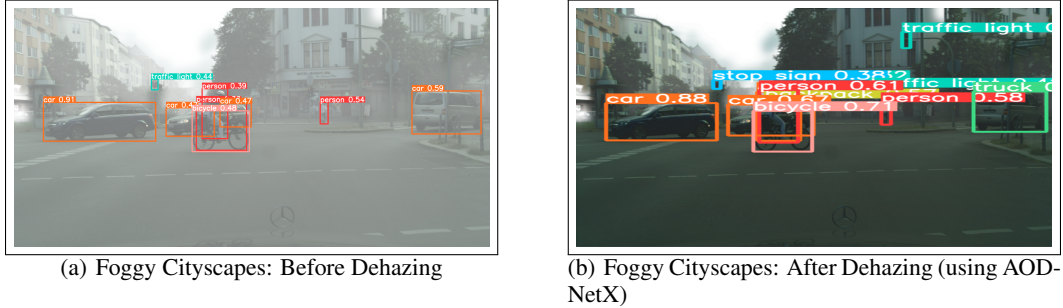


Figure 5: Dehazing performance on Foggy Cityscapes dataset.

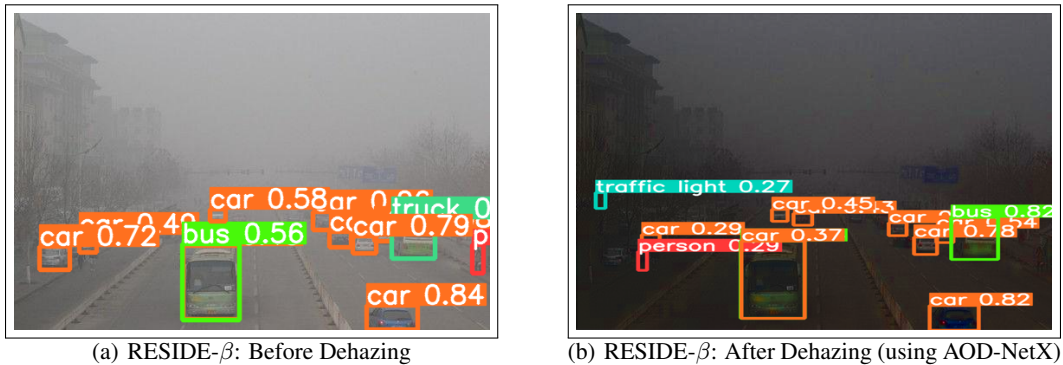


Figure 6: Dehazing performance on RESIDE- β dataset.

$$\text{MSE} = \frac{1}{mn} \sum_{i=0}^{m-1} \sum_{j=0}^{n-1} (I(i, j) - K(i, j))^2, \quad (3)$$

where $I(i, j)$ represents the pixel value at position (i, j) in the original image, and $K(i, j)$ represents the pixel value at the same position in the reconstructed image. Higher PSNR values generally indicate better reconstruction quality, as they imply a lower MSE and thus less distortion. PSNR is particularly useful for comparing the performance of different image processing algorithms in tasks such as image compression, denoising, and super-resolution.

G.2.1 MEAN AVERAGE PRECISION (mAP)

For object detection performance, we are using mean Average Precision (mAP):

$$AP = \frac{\sum_{k=1}^n (P(k) \times \text{rel}(k))}{\text{number of relevant documents}} \quad (4)$$

where:

- $P(k)$ is the precision at cutoff k in the list.
- $\text{rel}(k)$ is an indicator function equaling 1 if the item at rank k is a relevant document, 0 otherwise.
- n is the number of retrieved documents.

The mean Average Precision is then calculated as:

$$mAP = \frac{\sum_{q=1}^Q AP_q}{Q} \quad (5)$$

where AP_q is the Average Precision for the q^{th} query and Q is the total number of queries.